A Study of Multi-Phase Injection on Accelerating Crystal Oscillator Start-Up

Alireza Karimi-Bidhendi, *Member, IEEE*, and Payam Heydari, *Fellow, IEEE*

***Abstract*—As a widely used reference signal generator in communication systems, a crystal oscillator (XO) exhibits an unduly long start-up time T_S. External signal injection is an effective method to kick-start the XOs. However, the deviation from ideal injection frequency, which easily occurs and is hardly controllable, limits its effectiveness. This work analyzes the XO start-up behavior when differentially excited by an external oscillator and introduces a multi-phase signal injection method to mitigate the shortcomings of conventional injection techniques. Simulation results of an XO designed in a 180 nm CMOS process show that the proposed technique is capable of lowering T_S close to minimum theoretical limit.**

***Index Terms*—Crystal oscillators, series RLC, Hilbert transform, motional current, start-up, signal injection.**

I. Introduction

THE UBIQUITOUS use of sensing/communication devices in applications such as Internet of Things (IoT) has led to the emergence of design techniques to reduce the power consumption of all constituent building blocks within these devices. A crystal oscillator (XO) is often an indispensable part of these devices and is used as reference frequency generator or data converters' clock signal. However, the XO's long start-up time, T_S, and high start-up energy, E_S, limits the system latency and raises the stand-by power consumption.

One approach to reduce T_S involves boosting the negative resistance, R_N, presented to crystal by modifying the loading capacitor and amplifier's gain. This method was pursued by a number of prior arts [1], [2], [3]. However, increasing amplifier's gain may increase E_S. More importantly, the maximum achievable R_N is limited by crystal's static capacitor, C_0 [4]. To partially address the latter issue, [4] and [5] proposed methods to cancel C_0 by making the imaginary part of crystal's loading impedance inductive. References [6] and [7] employed multi-stage amplifiers to boost R_N without significant increase in the power consumption. The improvement provided by these techniques are limited due to various practical issues including process, voltage and temperature (PVT) variations, large power consumption of the assistant circuitry and its nonlinearities.

External signal injection using a ring or RC oscillator is an effective method to reduce T_S and has recently gained popularity. However, since crystal is a high Q-factor resonator, the injection frequency ω_{inj} needs to be sufficiently close (e.g., within $\pm 0.25\%$) to the crystal's series resonance frequency ω_S across PVT variations for this technique to be effective. Reference [8] implemented a precisely-timed injection method to lower T_S by properly adjusting the injection stop time such that crystal is not over or under energized. The low oscillation amplitude of 0.2 V in [8] further relaxes the accuracy of ω_{inj} at the cost of inferior phase noise [9]. Precise frequency injection methods were presented in [10] and [11] by one-time calibration of a ring oscillator (RO) using the XO at the system's start-up and saving the setting for future injection cycles. To relax the accuracy requirement of the injection oscillator, [12] and [13] proposed frequency dithering schemes, which effectively spread the injection power over a wide frequency range covering ω_S. For further robustness to PVT, various implementations of chirp signal injection have been introduced in [2] and [5], where the frequency is swept across a wide range over time. This added level of robustness, however, comes at the cost of lower deliverable energy to the crystal and thus a longer T_S. In [9], a signal injection technique was proposed in three steps. First, a coarsely-tuned open-loop RO started the XO with a small amplitude. In the second step, this RO was placed in a phase-locked loop (PLL) and locked to the XO. In the third step, the RO operated in an open loop fashion for a brief period before its frequency drifted from its locked state to drive the XO to its steady-state amplitude. Although effective, the complexity of this design may hinder its usage. In [14], a synchronized signal injection technique was employed to continuously drive the crystal till the desired oscillation amplitude is reached. Both [9] and [14] require the injection to be halted momentarily to either lock a PLL or re-calibrate the injection phase, which ultimately restrains these techniques to reach the theoretical lower limit of T_S. Reference [15] proposed a self-timed energy injection technique without explicit incorporation of an external injection oscillator. A relaxation oscillation behavior was realized based on the detection of i_M zero-crossings, and as such, injection frequency close to ω_S was achieved. A T_S of 6 μs was reported for a 50 MHz crystal with a 0.32 V differential voltage amplitude. In our prior work [4], we designed a relaxation oscillator (RXO) for precise frequency generation. Measurements showed this technique alone can lower T_S by $\sim 11\times$ compared to the XO's normal start-up. An analysis was also provided to evaluate crystal's motional current envelope, $i_{M,env}$, under injection.

This brief extends the concept of conventional single-phase signal injection, studied in [4], to multi-phase signal injection (MPSI). It is quantitatively shown that MPSI can bring the XO's start-up time down to its theoretical minimum, $T_{S,min}$, derived in [4]. As a proof of concept, two examples, namely, 2- and 4-phase injections are analyzed and simulated. The

Manuscript received November 25, 2019; revised February 5, 2020; accepted February 29, 2020. Date of publication March 3, 2020; date of current version November 24, 2020. This work was supported by the National Science Foundation Frontier Award under Grant 1646275. This brief was recommended by Associate Editor L. A. B. G. Oliveira. *(Corresponding author: Payam Heydari.)*

The authors are with the Department of Electrical and Computer Engineering, University of California at Irvine, Irvine, CA 92697 USA (e-mail: akarimib@uci.edu; payam@uci.edu).

Color versions of one or more of the figures in this article are available online at https://ieeexplore.ieee.org.

Digital Object Identifier 10.1109/TCSII.2020.2978097

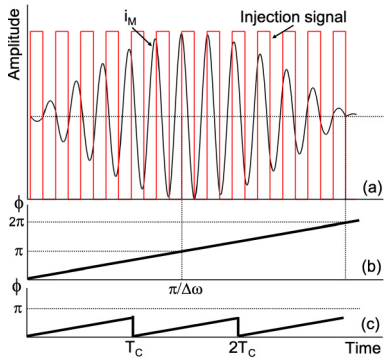

Fig. 1. (a) i_M and injection oscillator signal over time (b) accumulating ϕ causing injection oscillator to dampen i_M after $\pi/\Delta\omega$ (c) periodically "resetting" ϕ avoids the dampening of i_M.

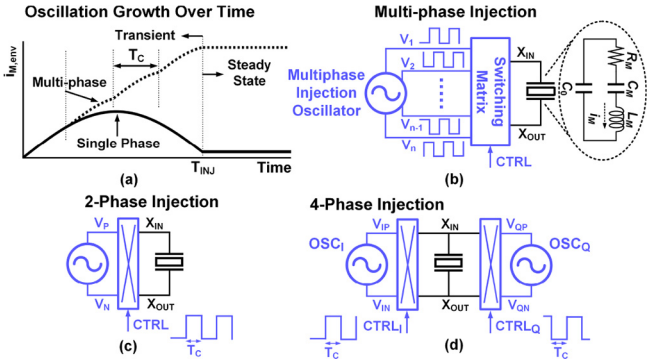

Fig. 2. Top level of MPSI technique (a) general block diagram, (b) $i_{M,env}$ under conventional injection and MPSI, (c) MPSI using 2 phases, (d) MPSI using 4 phases.

designs utilize the same RXO implemented and measured in [4] with addition of logic gates and switches, and tuned to 14 MHz.

II. Multi-Phase Signal Injection Analysis

The inevitable mismatch between ω_{inj} and ω_S creates an accumulating phase difference ϕ between crystal resonance and the injection oscillator's signal, resulting in a cyclic behavior of $i_{M,env}$ [4]. A qualitative explanation of this behavior is as follows: At $t = 0$, $\phi = 0$, and the injection oscillator constructively builds up the XO oscillation amplitude till $\phi = \pi$. Once $\phi = \pi$, the injecting signal starts counteracting the crystal resonance, i.e., damping the oscillation [*cf.* Fig. 1(a) and (b)]. To address this fundamental issue, we introduce MPSI as a mechanism that causes ϕ to periodically reset to zero (*see* Fig. 1(c)). Rotation between multiple phases of the injection oscillator with a phase separation of θ with respect to one another after a specific injection duration T_C compensates for this excess phase difference ϕ, thus re-aligning the crystal resonance and injecting signal. The perfect realignment occurs if $\phi = \theta$. The injection duration T_C varies depending on the rate of phase accumulation $\Delta\omega$ (i.e., $\Delta\omega = 2\pi\Delta f \simeq \omega_{inj} - \omega_S$) and the number of phases, N, in this multi-phase oscillator. For example, for a quadrature injection oscillator, $N = 4$ and ϕ is reset once $\phi = \pi/2$, translating to $T_C = \pi/2\Delta\omega$. The total injection time T_{INJ} is equal to $N \times T_C$. Consider a crystal with an initial condition, driven differentially in the k-th injection duration by phase θ_k of a multi-phase injection oscillator that produces a periodic square pulse with an amplitude of $V_{DD} =$ 1.8 V. The governing ordinary differential equation and initial conditions are:

$$\begin{aligned} \frac{4V_{DD}\omega_{inj}}{\pi L_M}\cos\left(\omega_{inj}t + \theta_k\right) &= \frac{d^2 i_M}{dt^2} + 2\alpha\frac{di_M}{dt} + \omega_S^2 i_M \\ i_M(t = (k-1)T_C) &= i_M(k-1), \\ \frac{di_M}{dt}(t = (k-1)T_C) &= i'_M(k-1) \end{aligned} \tag{1}$$

where $\alpha = R_M/2L_M$, $\omega_S = 1/\sqrt{L_M C_M}$ and k is an integer from 1 to N. R_M, C_M and L_M are crystal's motional resistor, capacitor and inductor. As an example, a 14 MHz crystal is used in this brief with $C_M = 11.75$ fF, $L_M = 10.996$ mH, $R_M = 25\ \Omega$, $C_0 = 3$ pF, and is loaded with $C_S = 10$ pF.

Following the approach in [4] and considering the practical case where $\Delta\omega \gg \alpha$ (see [4]), the steady-state solution of this differential equation is readily derived:

$$i_{M,ss}(t) = I_{inj}\left[x(t)\cos\omega_d t + y(t)\sin\omega_d t\right] \tag{2}$$

where:

$$\begin{aligned} I_{inj} &= \frac{2V_{DD}}{\pi L_M \Delta\omega}\left(1 - \frac{\Delta\omega}{\omega_d}\right),\ \ \omega_d = \sqrt{\omega_S^2 - \alpha^2} \\ x(t) &= z(t)\sin\theta_k - w(t)\cos\theta_k, \\ y(t) &= z(t)\cos\theta_k - w(t)\sin\theta_k \\ z(t) &= \alpha\cos\Delta\omega t + \Delta\omega\sin\Delta\omega t - \alpha e^{-\alpha t} \\ w(t) &= \alpha\sin\Delta\omega t + \Delta\omega\cos\Delta\omega t - \Delta\omega e^{-\alpha t} \end{aligned} \tag{3}$$

The transient solution due to initial condition for $i_M(t)$ is readily shown to be:

$$\begin{aligned} i_{M,t}(t) &= \Bigg[i_M(k-1)\cos\omega_d t \\ &\qquad + \frac{\alpha i_M(k-1) + i'_M(k-1)}{\omega_d}\sin\omega_d t\Bigg] e^{-\alpha t} \\ &\simeq i_M(k-1)e^{-\alpha t}\cos\omega_d t \end{aligned} \tag{4}$$

The second term in $i_{M,t}(t)$ is negligible compared to the first, because $\omega_d \gg \alpha$ (by four orders of magnitude). The overall response $i_M(t)$ is derived by summing up the steady-state and transient responses of (2) and (4). To evaluate the stored energy in the crystal in the k-th injection duration, $i_{M,env}$, which is an indicator of crystal's start-up behavior, is derived:

$$i_{M,env}(t) = I_{inj}\sqrt{\left(x(t) + i_M(k-1)e^{-\alpha t}/I_{inj}\right)^2 + y(t)^2} \tag{5}$$

From (5), it is evident that C_0 does not have an effect on $i_{M,env}$, while crystal's Q-factor inversely affects it. Prior to the first injection duration, i.e., $k = 1$, thermal noise provides a negligible initial condition to crystal and therefore $i_M(0) = 0$. For each subsequent injection duration, the initial condition is equal to $i_{M,env}$ at the end of the preceding period.

Fig. 2(a) depicts $i_{M,env}(t)$ under conventional single-phase injection (in solid) and MPSI (in dash), demonstrating its continual growth with the latter. Fig. 2(b) shows top-level realization of MPSI. A switching matrix selects proper phases of the oscillator to be applied to crystal. In Fig. 2(c), a 2-phase version of MPSI is shown in which the switch block alternates the connection polarity between RXO and crystal every T_C seconds. In Fig. 2(d), a quadrature RXO drives crystal through two switching blocks which are enabled by quadrature controlled signals ($CTRL_I$ and $CTRL_Q$). Fig. 3 shows the $i_{M,env}$ growth based on the closed form expression in (5) for three techniques with equal total injection times. Conventional (or 1-phase) injection cannot grow $i_{M,env}$ above 0.7 mA and

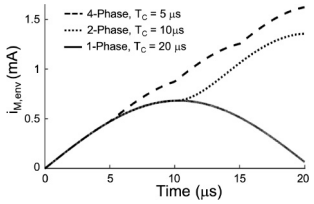

Fig. 3. $i_{M,env}$ compared for 3 injection techniques for $\Delta f = 50$ kHz.

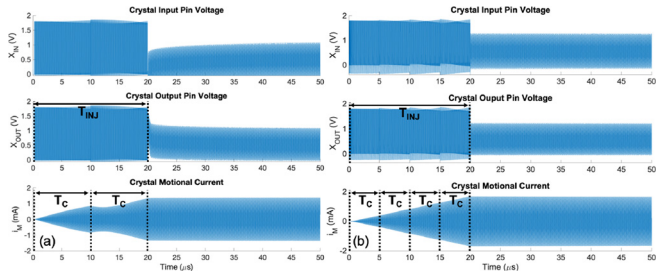

Fig. 4. XO's start-up sample simulations for (a) 2-phase and (b) 4-phase injection techniques.

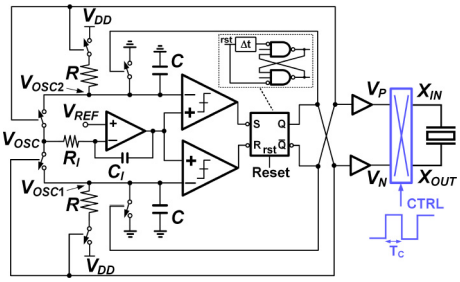

Fig. 5. Schematic of two-phase signal injection using RXO.

starts to counteract the resonance at $t = 10$ μs. The 4-phase design reaches higher $i_{M,env}$ at a faster rate (i.e., at a shorter T_S) than the 2-phase counterpart. Fig. 4 shows samples of circuits' simulation results under 2- and 4-phase injections. Both methods can drive the crystal close to its steady-state with the 4-phase injection delivering a higher energy to crystal. After injection, crystal is disconnected from RXO and is connected to an inverting amplifier for steady-state operation.

III. Two-Phase Signal Injection

The simplest form of MPSI utilizes two phases in which crystal is driven continuously for at least two equal durations. The schematic of this implementation is shown in Fig. 5 with the RXO introduced in [4]. For the startup to reach its minimum theoretical limit [4], the injection phase should be reversed once $i_{M,env}$ reaches its maximum during the first injection cycle at $t = \pi/\Delta\omega$. Therefore, at $t = \pi/\Delta\omega$, the injection phase of RXO is reversed using a pair of switches (Fig. 5). By the end of the second injection duration, crystal reaches the steady state – depending on crystal's Q-factor and frequency accuracy within which the RXO can generate oscillation – and injection is stopped. The RXO in this design is configured to operate at 14 MHz with < 0.3% frequency variation over –20 to 80 °C range after an initial calibration. It shows 1.8% frequency variation for supply variations over 1.7–1.8 V. This sensitivity can be alleviated by utilizing a low dropout voltage regulator without significant effects on XO's T_S or E_S. Given a very high crystal's Q-factor, injections may fail to help the crystal reach its steady-state over two periods.

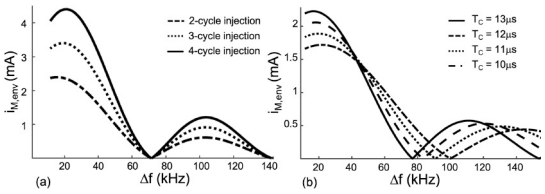

Fig. 6. (a) $i_{M,env}$ for 2-phase injection technique with T_C =14 μs at different cycles, (b) $i_{M,env}$ of 2-phase injection technique for various T_C.

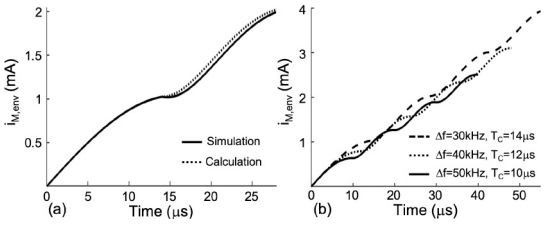

Fig. 7. (a) Calculated and simulated $i_{M,env}$ for 2-phase injection at $\Delta f =$ 30 kHz and $T_C = 14$ μs. (b) $i_{M,env}$ for 4 cycles of 2-phase injection.

In this case, one might continue the injection by periodically reversing the RXO phase over more injection cycles. However, doing so requires an RXO with better frequency stability to limit the variation of $i_{M,env}$ and subsequently T_S [*see* Fig. 6(a)]. In other words, a non-ideal resetting of ϕ leaves a residue phase that ultimately limits the number of injection durations. Fig. 6(b) demonstrates the $i_{M,env}$ magnitude variation vs. Δf for four injection durations T_C. It is inferred that a smaller T_C would relax the frequency stability requirement of the RXO at the expense of reaching a smaller $i_{M,env}$. Fig. 7(a) compares the $i_{M,env}$ magnitude obtained from simulation and closed form expression in (5) for a sample case where $\Delta f = 30$ kHz and $T_C = 14$ μs with a total injection time T_{INJ} of 28 μs, verifying a great agreement between the two. Fig. 7(b) shows that it is possible to reach large values of $i_{M,env}$ if crystal is driven over 4 injection durations using 2-phase technique.

To assess the performance of this method, we study a typical case: For an XO with the aforementioned crystal parameters and a steady-state voltage amplitude of $V_{osc} = 1.5$ V (equivalent to an $i_{M,env}$ of 1.7 mA), $T_{S,min} \simeq 15$ μs is calculated [4]:

$$T_{S,min} = \frac{2L_M}{R_M} ln\left(1 - \frac{\pi R_M}{4V_{DD}} \times 0.9(C_S + C_0)\omega_{osc} V_{osc}\right)^{-1} \quad (6)$$

where ω_{osc} is the steady-state oscillation frequency. For a $T_C =$ 11 μs and over 2 cycles, Eq. (5) predicts that the 2-phase injection reaches 90% of steady-state amplitude in 22 μs given a 0.3% frequency stability for RXO. In other words, the crystal starts very quickly in 308 oscillation cycles.

IV. Four-Phase Signal Injection

An alternative MPSI is realized by rotating the RXO phase when $\phi = \pi/2$ or equivalently $t = \pi/2\Delta\omega$. In order to implement this method, a quadrature injection oscillator is required. In this brief, we leverage the RXO attribute in generating higher precision oscillation compared to a ring oscillator and propose a novel quadrature RXO (QRXO), shown in Fig. 8. Designed to operate at 14-MHz, it is composed of 2 coupled RXO's. The start-up sequence and operation of the QRXO is explained, as follows (*see* Fig. 9).

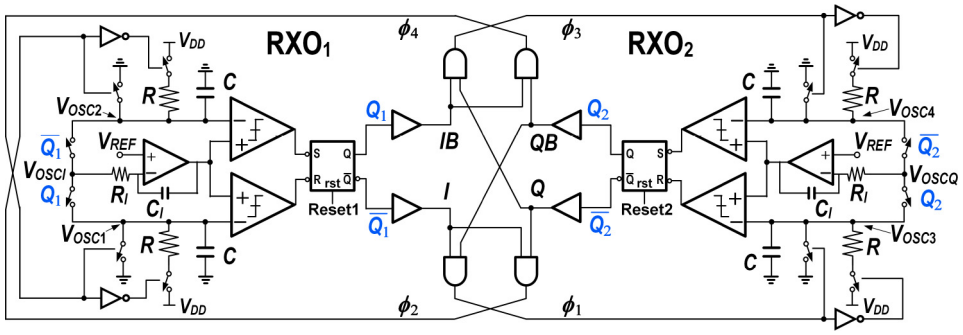

Fig. 8. Quadrature RXO schematic.

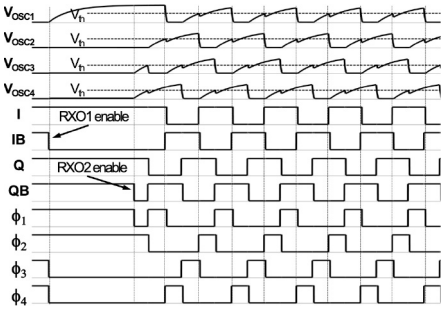

Fig. 9. Timing diagram of QRXO.

1) Initially, both inputs of NAND-based SR latches are pulled low and their outputs are high. One of the RXOs, e.g., RXO_1, is released first from the reset state and due to (intentional) internal delay between NANDs' input $Q_1 = IB = 0$. Consequently, $\phi_3 = \phi_4 = 0$ and V_{OSC1} starts charging up.

2) All outputs hold their states afterwards until RXO_2 is released resulting in $Q_2 = QB = 0$ and subsequently $\phi_1 = 0$. V_{OSC3} and V_{OSC4} start charging up together.

3) When V_{OSC3} and V_{OSC4} pass the comparator threshold V_{th}, the latch will briefly enter the invalid mode ($S = R = 0$) and $Q = QB = 1$. This makes $\phi_1 = 1$.

4) Steady-state operation: once $\phi_1 = 1$, V_{OSC3} is shorted to GND. However, invalid state of the RXO_2's latch causes V_{OSC3} and V_{OSC4} to be shorted. Thus, a brief drop in V_{OSC4} occurs before the latch returns to a valid state and makes $\overline{Q_2} = Q = 0$. As a result, $\phi_2 = 0$ and V_{OSC2} starts charging.

5) When $V_{OSC2} > V_{th}$, $IB = 1$ and ϕ_4. RXO_1's latch briefly enters invalid mode shorting V_{OSC1} and V_{OSC2} while V_{OSC1} is discharging to GND. Once $V_{OSC1} < V_{th}$, $\overline{Q_1} = I = 0$. Next, $\phi_1 = 0$ and V_{OSC3} starts charging.

6) Similar process will occur in RXO_2 and again back in RXO_1, resulting in the quadrature outputs. Note that the internal nodes ϕ_1–ϕ_4 oscillate with a 25% duty cycle.

A similar operation will be deducted if RXO_2 starts first, which results in the exact steady-state waveform with Q leading I. The QRXO shows a simulated frequency stability of $< \pm 0.1\%$ over –20 to 80 °C range and settles within 0.1% of the steady-state frequency in <1.4 μs. It shows 1.9% frequency variation for supply variations over 1.7–1.8 V. It dissipates 85 nJ over a 20 μs injection period. Fig. 10 shows the variation of $i_{M,env}$ vs. Δf for four injection durations. It is possible to reach a high $i_{M,env}$ if frequency stability is better than 0.4%. For instance, the same XO in previous section with $T_{S,min} = 15$ μs can reach its steady-state in 20 μs with a $T_C = 5$ μs. $i_{M,env}(t)$ derived from analytical study in Section II and circuit simulation is shown in Fig. 11(a) at a sample Δf and T_C. Fig. 11(b) shows $i_{M,env}$ behavior over time for various Δf

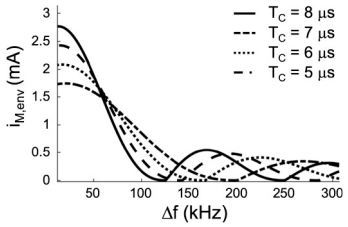

Fig. 10. Calculated $i_{M,env}$ of 4-phase injection technique for various T_C.

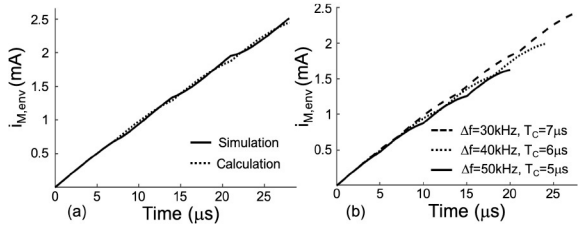

Fig. 11. (a) Calculated and simulated $i_{M,env}$ for 4-phase injection technique at $\Delta f = 30$ kHz and $T_C = 7$ μs (b) $i_{M,env}$ for sample Δf and T_C values.

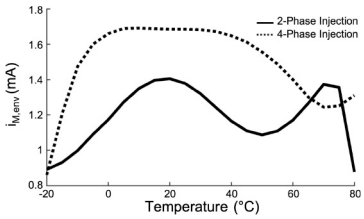

Fig. 12. Simulated $i_{M,env}$ at the end of MPSI period over temperature.

and T_C values. A lower Δf allows for a longer T_C to reach a higher oscillation amplitude.

V. Design Considerations

To lower T_S variation across temperature, injection oscillator's frequency has to calibrated such that its frequency is always larger (or always smaller) than ω_d over temperature. If this condition is not met, the injection over subsequent cycles may counteract crystal resonance at the temperature where $\omega_d - \omega_{inj}$ changes sign. Fig. 12 shows the simulated $i_{M,env}$ at the end of injection over temperature as an indicator for variation in T_S. $i_{M,env}$ fluctuates by ±14% over 100 °C temperature variation, resulting in $\simeq$20% variation of T_S over the same range. Fig. 13(a) compares the sensitivity of conventional, 2- and 4-phase techniques to Δf for an equal total injection time. The 4-phase injection technique exhibits the smallest frequency stability requirement. Equivalently, using 4-phase technique results in a higher $i_{M,env}$, as shown in Fig. 13(b). A

TABLE I
PERFORMANCE SUMMARY AND COMPARISON WITH PRIOR ART

	[2]	[12]	[1]	[5]	[8]	[9]	[14]	[15]	[7]	[13]	[4]	This Work[1]
CMOS process (nm)	180	65	90	65	65	65	55	22 FD-SOI	65	130	180	180
Core area (mm^2)	0.12	0.08	0.072	0.023	0.09	0.069	0.049	0.02	0.0053	0.058	0.108	N/A
Supply (V)	1.5	1.68	1	0.35	1	1	1.2	0.8	1.2	1.2	1	1.8
Frequency (MHz)	39.25	24	24	24	50	54	32	50	40	32	48	14
Load capacitor C_L (pF)	6	6	10	6	9	6	6	7	9	10	8	10
Steady-state amplitude (V)	1.5	N/A	N/A	0.3	0.2	0.7	0.37	0.16	N/A	N/A	0.7	1.5
PN (dBc/Hz) at 1 kHz	-147	N/A	N/A	-134	N/A	-139.5	N/A	-123	N/A	N/A	-135	-136
Steady-state power (μW)[1]	181	393	95	31.8	195	198	190	51	141	181.6	180	198
Start-up time T_S (μs)	158	64	200	400	2.2	19	23	6	64	32.7	18	22 ❙ 20
T_S (cycles)	6162	1536	4800	9615	110	1026	736	300	2560	1046	864	308 ❙ 280
T_S improvement ratio	13.3×	6.7×	13.3×	3.3×	N/A	31.5×	17.4×	N/A	17.3×	N/A	102.7×	89× ❙ 107×
Start-up energy E_S (nJ)	349	N/A	36	14.2	13.3	34.9	20.2	3.7	37.2	31.7	114.5	59 ❙ 85
E_S improvement ratio	1.1×	N/A	6.9×	2.8×	N/A	N/A	N/A	N/A	4.1×	N/A	2.9×	7.2× ❙ 5×
ΔT_S over Temp. (%)	7	±35	27.5	7.5	7	±1.25	±10	23	±10	N/A	±12	∼ ±20
Temp. range (°C)	-30–125	-40–90	-40–90	-40–90	-40–90	-40–85	-40–140	-40–85	-20–85	-20–100	-40–90	-20–80
Start-up technique	Chirp injection g_m-boost	Dithered injection	Dynamic load, g_m-boost	g_m-boost Chirp injection	Precisely-timed injection	2-step injection	Sync. signal injection	Self-timed energy injection	g_m-boost	GSDI g_m-boost	PDI, AI	MPSI ϕ=2 ❙ ϕ=4

[1] Simulation results.

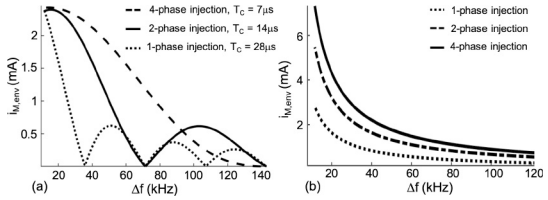

Fig. 13. (a) $i_{M,env}$ of 3 techniques for an equivalent total injection time showing sensitivity to Δf, (b) Effect of frequency inaccuracy on $i_{M,env}$ for 3 injection techniques given $T_C = \pi/\Delta\omega$, $T_C = \pi/2\Delta\omega$ and $T_C = \pi/4\Delta\omega$ for 1-phase, 2-phase and 4-phase injection techniques, respectively.

natural expansion of the MPSI technique is to use higher number of phases to start the XO. However, increased circuit complexity and higher power dissipation may offset the improvement in T_S. Additionally, some internal nodes of the injection oscillator operate at a duty cycle that is inversely proportional to the number of phases, N, requiring faster circuitry for a higher N. Table I summarizes the performance and compares it with prior art. MPSI can achieve the largest improvement ratio in T_S with a comparable E_S to other works. The designs in [8] and [15] report similar or smaller number of oscillation cycles it takes for the XO to start, however, this is achieved by targeting a small steady-state oscillation amplitude which results in a poor phase noise. Note that the $T_{S,min}$ corresponding to these works are smaller than 100 oscillation cycles.

VI. CONCLUSION

In this brief, MPSI was introduced to kick start the XO and improve T_S. An analytical study was carried out to evaluate the design specifications for the injection oscillator and design trade-offs. A new quadrature RXO was introduced to implement the 4-phase injection scheme. Simulations illustrated the effectiveness of this method, concluding XO reaches a large steady-state amplitude in less than 300 injection cycles, i.e., with a T_S close to $T_{S,min}$.

REFERENCES

[1] M. Ding *et al.*, "A 95μW 24MHz digitally controlled crystal oscillator for IoT applications with 36nJ start-up energy and >13× start-up time reduction using a fully-autonomous dynamically-adjusted load," in *IEEE Int. Solid-State Circuits Conf. Dig. Tech. Papers (ISSCC)*, Feb. 2017, pp. 90–91.

[2] S. Iguchi, H. Fuketa, T. Sakurai, and M. Takamiya, "Variation-tolerant quick-start-up CMOS crystal oscillator with chirp injection and negative resistance booster," *IEEE J. Solid-State Circuits*, vol. 51, no. 2, pp. 496–508, Feb. 2016.

[3] K.-M. Lei, P.-I. Mak, and R. P. Martins, "A 0.4V 4.8μW 16MHz CMOS crystal oscillator achieving 74-fold startup-time reduction using momentary detuning," in *Proc. IEEE Int. Symp. Circuits Syst.*, May 2017, pp. 1–4.

[4] A. Karimi-Bidhendi, H. Pu, and P. Heydari, "Study and design of a fast start-up crystal oscillator using precise dithered injection and active inductance," *IEEE J. Solid-State Circuits*, vol. 54, no. 9, pp. 1–12, Sep. 2019.

[5] K.-M. Lei, P.-I. Mak, M.-K. Law, and R. P. Martins, "A regulation-free sub-0.5-V 16-/24-MHz crystal oscillator with 14.2-nJ startup energy and 31.8-μW steady-state power," *IEEE J. Solid-State Circuits*, vol. 53, no. 9, pp. 2624–2635, Sep. 2018.

[6] S. Iguchi, A. Saito, Y. Zheng, K. Watanabe, T. Sakurai, and M. Takamiya, "93% power reduction by automatic self power gating (ASPG) and multistage inverter for negative resistance (MINR) in 0.7V, 9.2μW, 39MHz crystal oscillator," in *Proc. IEEE Symp. VLSI Circuits*, Jun. 2013, pp. C142–C143.

[7] M. Miyahara, Y. Endo, K. Okada, and A. Matsuzawa, "A 64μs start-up 26/40MHz crystal oscillator with negative resistance boosting technique using reconfigurable multi-stage amplifier," in *Proc. IEEE Symp. VLSI Circuits*, Jun. 2018, pp. 115–116.

[8] H. Esmaeelzadeh and S. Pamarti, "A quick startup technique for high-Q oscillators using precisely timed energy injection," *IEEE J. Solid-State Circuits*, vol. 53, no. 3, pp. 692–702, Mar. 2018.

[9] K. M. Megawer *et al.*, "A fast startup CMOS crystal oscillator using two-step injection," *IEEE J. Solid-State Circuits*, vol. 54, no. 12, pp. 3257–3268, Dec. 2019.

[10] B. Lleveland, "Fast startup resonant element oscillator," U.S. Patent US2 009 001 534 2A1, Jan. 15, 2009.

[11] Y.-I. Kwon, S.-G. Park, T.-J. Park, K.-S. Cho, and H.-Y. Lee, "An ultra low-power CMOS transceiver using various low-power techniques for LR-WPAN applications," *IEEE Trans. Circuits Syst. I, Reg. Papers*, vol. 59, no. 2, pp. 324–336, Feb. 2012.

[12] D. Griffith, J. Murdock, and P. T. Røine, "A 24MHz crystal oscillator with robust fast start-up using dithered injection," in *IEEE Int. Solid-State Circuits Conf. Dig. Tech. Papers (ISSCC)*, Jan. 2016, pp. 104–105.

[13] M. Scholl *et al.*, "A 32 MHz crystal oscillator with fast start-up using dithered injection and negative resistance boost," in *Proc. IEEE 45th Eur. Solid State Circuits Conf. (ESSCIRC)*, Sep. 2019, pp. 49–52.

[14] B. Verhoef, J. Prummel, W. Kruiskamp, and R. Post, "A 32MHz crystal oscillator with fast start-up using synchronized signal injection," in *IEEE Int. Solid-State Circuits Conf. Dig. Tech. Papers (ISSCC)*, Feb. 2019, pp. 304–305.

[15] J. B. Lechevallier, R. A. R. Van Der Zee, and B. Nauta, "Fast & energy efficient start-up of crystal oscillators by self-timed energy injection," *IEEE J. Solid-State Circuits*, vol. 54, no. 11, pp. 3107–3117, Nov. 2019.